

SBS 0909+532: A New Double Gravitational Lens or Binary Quasar? ^{1 2 3}

Christopher S. Kochanek

Emilio E. Falco

Rudolf Schild

Adam Dobrzycki

Harvard-Smithsonian Center for Astrophysics
60 Garden Street
Cambridge MA 02138

Dieter Engels

Hans-Jürgen Hagen
Hamburger Sternwarte
Gojenbergsweg 112, D-21029 Hamburg
Germany

ABSTRACT

The $z = 1.377$, $B = 17.0$ mag quasar SBS 0909+532 A, B is a double with two images separated by $\Delta\theta = 1''.107 \pm 0''.006$. Because the faint image has an emission line at the same wavelength as the MgII 2798 Å emission line of the quasar, and lacks the broad MgIb absorption feature expected for a star with the same colors (a K star), we conclude that image B is a quasar with similar redshift to image A. The relative probabilities that the double is the smallest separation ($4.8h^{-1}$ kpc for $\Omega_0 = 1$) correlated quasar pair or a gravitational lens are $\sim 1 : 10^6$. If the object is a lens, the mean lens redshift is $\langle z_l \rangle = 0.5$

¹Observations reported here were obtained, in part, at MDM Observatory, a consortium of the University of Michigan, Dartmouth College and the Massachusetts Institute of Technology.

²This research made use of the NASA/IPAC Extragalactic Database (NED) which is operated by the Jet Propulsion Laboratory, Caltech, under contract with the National Aeronautics and Space Administration

³We have made use in part of finder chart(s) obtained using the Guide Stars Selection System Astrometric Support Program developed at the Space Telescope Science Institute (STScI is operated by the Association of Universities for Research in Astronomy, Inc., for NASA)

with 90% confidence bounds of $0.18 < z_l < 0.83$ for $\Omega_0 = 1$. If the lens is an elliptical galaxy, we expect it to be brighter than $I < 19.5$ mag. The broad band flux ratio varies with wavelength, with $\Delta I = 0.31$, $\Delta R = 0.58$, and $\Delta B = 1.29$ magnitudes, which is difficult to reconcile with the lensing hypothesis.

Subject headings: Gravitational Lenses

1. Introduction

Gravitational lenses offer the best current constraint on the cosmological constant, with a current upper limit of $\lambda_0 < 0.65$ at 2σ in flat cosmological models (Kochanek 1996). The uncertainties in the limit are still dominated by Poisson uncertainties due to the small number of gravitational lenses available for the analysis. We have been conducting a survey for gravitationally lensed quasars (Kochanek, Falco & Schild 1995) to reduce these uncertainties. Here we report on the first new lens candidate found in our sample.

SBS 0909+532 was identified in the course of the Hamburg-CfA Bright Quasar Survey (Engels et al. 1996). The quasar was discovered by Stepanyan et al. (1991), with coordinates accurate to $\sim 1'$ (see also Véron-Cetty & Véron 1996). Our astrometric solution based on GSC stars in the field yields $\alpha = 9:13:00.76$, $\delta = +52:59:31.5$ (J2000), with an uncertainty of $\sim 1''$. The object was recognized as a blue object on an objective prism plate taken with the Calar Alto Schmidt telescope, and subsequent spectroscopy with the Tillinghast 1.5m telescope at FLWO (Fred Lawrence Whipple Observatory) on Mt. Hopkins confirmed it to be a quasar. SBS 0909+532 was included in the FKS survey for gravitationally lensed quasars (Kochanek, Falco & Schild 1995) because of its redshift ($z = 1.377$) and bright optical flux ($m_B \sim 17$ mag). The quasar was first imaged on 19 November 1995 in $2''.9$ FWHM seeing on the 1.2m FLWO telescope on Mt. Hopkins. The results were consistent with a point source, but, because of the poor seeing conditions of the observation, the quasar was returned to the survey observation list. The next observation was on 13 January 1996 in $1''.2$ FWHM seeing on the MDM (Michigan-Dartmouth-MIT) 2.4m telescope. The object was visibly extended, and an analysis using Daophot (Stetson 1992) split it into a double with a separation of $\Delta\theta = 1''.1$ and flux ratio of $0.58 R$ mag.

Subsequent efforts focused on determining whether both components were quasars. In §2 we detail our photometric observations of the system, including narrow-band filters bracketing the MgII 2798 Å line of the quasar. In §3, we detail our spectroscopic observations, and in §4 we discuss whether SBS 0909+532 A, B is a gravitational lens or the smallest known binary quasar.

2. Photometry

Following the identification of SBS 0909+532 as a double, on 25 January 1996 P. Schechter obtained multiple 60-second exposures of the quasar with the MDM 2.4m telescope in the I , R filters and 120-second exposures in the B filter. The seeing conditions ranged from $0''.95$ to $1''.60$ FWHM. During that night, we also obtained exposures in I , R

and B of the Landolt photometric standard stars PG1323-086, PG1323-086A, PG1323-086C and PG1323-086B. We used these stars to determine that conditions were photometric, and to calibrate the magnitudes of the quasars. The quasar exposures were kept short so that the brighter stars near the quasar would be unsaturated and could be used as psf templates. The detector was a thinned CCD (“Charlotte”) with pixel scale $0.^{\circ}275$, gain $3.45 \text{ e}^-/\text{ADU}$, and read noise of 4e^- . Figure 1 shows a $\sim 3'$ field containing SBS 0909+532, including the nearby stars labeled a, b, and c that we used as psf templates and in spectroscopic tests. Figure 2 shows our highest resolution B , R and I images.

Each image was processed using Daophot (Stetson 1992) to determine the positions and fluxes of the two components. The calibrated magnitudes of the A (bright) and B (faint) components are listed in Table 1; their inferred separations and flux ratios are summarized in Table 2. We neglect galactic extinction, which is less than $E(B - V) < 0.03$ (Burstein & Heiles 1982). In all cases, the quasar is separable into two components, although in the worst-seeing I image ($1.^{\circ}6$ FWHM) the separation is not well determined. We discard this image from the subsequent analysis.

After several attempts to obtain independent spectra of the A and B components failed due to poor seeing or ambiguities produced by differential refraction (see §3), we decided to use narrow-band filters to search for the MgII 2798 Å emission line redshifted to 6651 Å. On 11-13 April 1996 we obtained narrow-band images with the MDM 2.4m telescope in $0.^{\circ}95$ to $1.^{\circ}20$ FWHM seeing, in 3 redshifted H α filters (see Table 3 for their properties). We acquired 6-minute exposures with the $KP6520$ and $KP6737$ filters, and 10-minute exposures with the $KP6649$ filter. The detector was a thick CCD (“Nellie”) with pixel scale $0.^{\circ}241$, gain $2.95 \text{ e}^-/\text{ADU}$, and read noise of 4e^- . Unfortunately, we had no comparable filter sequence for the stronger CIV 1549 Å or CIII] 1909 Å lines at 3682 Å and 4538 Å.

We processed the narrow-band images with Daophot, in the same manner as the broad-band images. The component separations (see Table 2) found for all six filters and the two different cameras are mutually consistent; we find a best estimate for the separation of $\Delta\theta = 1.^{\circ}109 \pm 0.^{\circ}006$ for the Charlotte chip and $1.^{\circ}102 \pm 0.^{\circ}007$ for the Nellie chip, where the uncertainties are the observed scatter in the separations found for the individual images and the difference between the two chips is probably due to 1% errors in the chip scales. We tested the plausibility of the uncertainties using Monte Carlo simulations. For the best I images, the expected statistical uncertainties in the position and flux were $0.^{\circ}002$ and 0.001 mag respectively, so the observed uncertainties are dominated by systematic errors. The position angle of B relative to A is $115.^{\circ}2 \pm 0.^{\circ}3$ (E of N).

In Figure 3 we combine the calibrated total spectrum (see §3) with the relative photometry to illustrate the broad features of the spectra of components A and B and

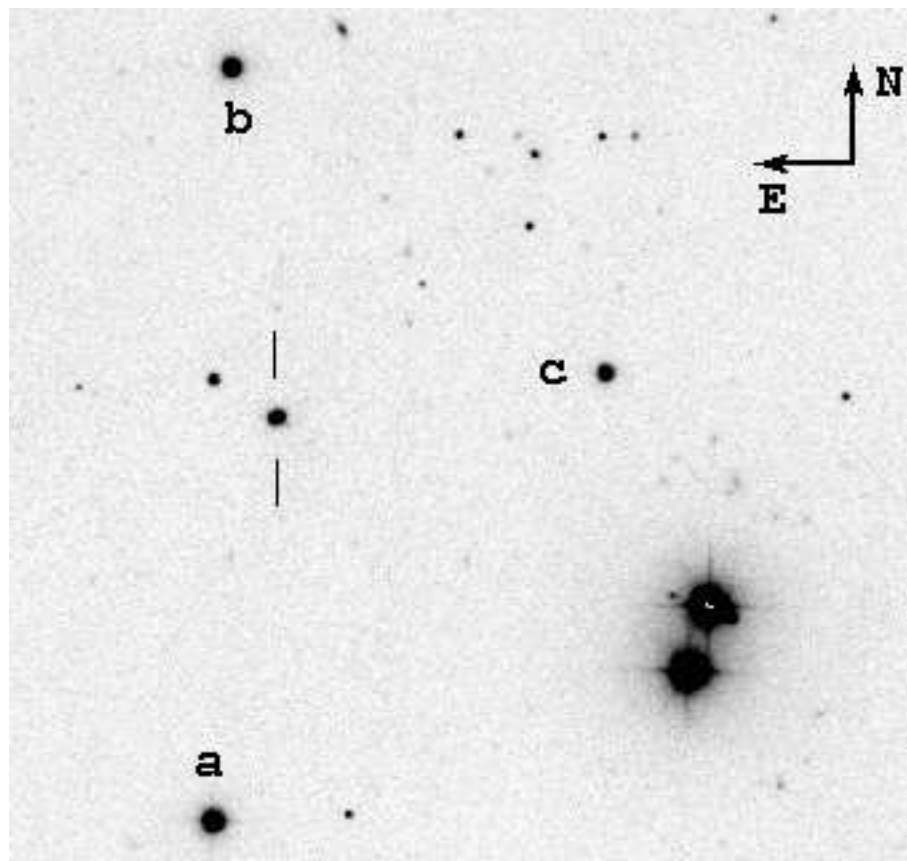


Fig. 1.— Stacked I images of SBS 0909+532 A, B, showing a $\sim 3'$ field containing the quasar, indicated by the half-cross-hair. The length of the arrows is $20''$.

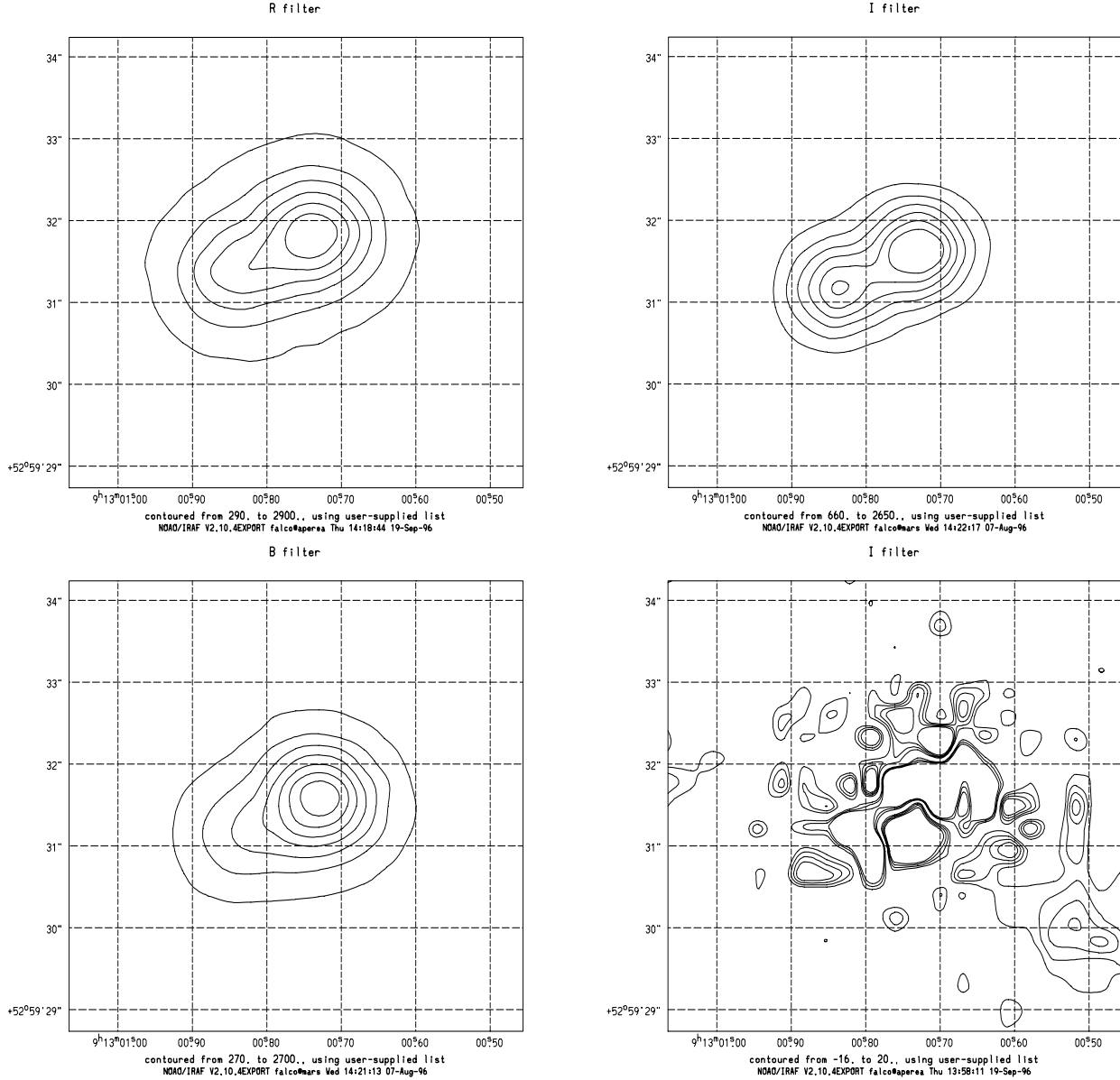


Fig. 2.— Close-up views of our best-seeing B , R and I images of SBS 0909+532 A,B and of the residuals after subtraction of A and B from the I stack of Fig. 1 (clockwise from left, bottom). The coordinates are J2000. The A (B) component is on the right (left). The image contours are spaced by $\sim 15\%$ from the A maximum values. The residual contours are spaced by 2σ between -4 and $+8\sigma$, where the peak in the stacked I image is $\sim 650 \times \sigma$ and σ is the sky noise level. The dominant features near the locations of A and B are due to imperfect subtractions. The faint object $\sim 2\text{''}2$ SW of A and B is a possible galaxy that may be the absorber at $z \sim 0.83$ (see text). This object is present, but barely discernible in Fig. 1.

for star c. The MgII 2798 Å line is clearly apparent above the *R* continuum in both components. The contrast between the on-line (KP6649) and off-line (KP6520 and KP6737) filters is -0.32 ± 0.05 mag in the bright quasar component, and -0.21 ± 0.04 mag in the fainter quasar component. The continuum on either side of the line is flat, with a slope of 0.002 ± 0.055 mag between the KP6520 and KP6737 filters (see Table 2), and slightly bluer than the average *R* flux. The equivalent width of the MgII 2798 Å line is smaller in component B than in component A, because the flux ratio in the KP6649 line filter is 0.13 ± 0.01 mag greater than in the two off-line filters. The broad band colors of component B are consistent with a K4 star, but K stars lack strong emission or absorption features in the wavelength range of the KP 6649 filter. For example, star b has the colors of a K3 star, but shows no line feature in the narrow band filters. A cooler M star could produce features in the narrow band filters. For example, star c is an M3 star, and we see the edge of one of the molecular absorption bands in the narrow band filters (see Figure 3). Note, however, that we see a gradient in the narrow band filters with the KP 6520 filter above the *R* continuum, the KP 6649 filter on it, and the KP 6737 filter below it, rather than the line feature seen in components A and B. We conclude that both A and B are quasars at comparable redshifts, but that the equivalent width of the MgII 2798 Å line is smaller in B than in A.

3. Spectroscopy

We made three attempts to spectroscopically resolve the two objects, with mixed success due to poor seeing during each of the observations. We report only on the best of these observations. On 22 April 1996, we obtained long slit spectra of the quasar with a $1'' \times 180''$ slit parallel to the component separation. We used the MMT with the Blue Channel spectrograph and a Loral 3K×1K CCD. With the same slit in the same orientation, we obtained spectra of star c just before and after the spectrum of the quasar. The spatial scale of the image is $0''.30$ per pixel, the wavelength scale is 1.96 Å/pixel, the gain is 1.5 and the read noise $7.5 e^-$. The seeing during the observations was $1''.9$ FWHM; the spectral resolution was ~ 6.5 Å FWHM. In the resulting spectrum, the two components of the SBS 0909+532 system are not separable by standard reduction methods. On 20 April 1996, we had obtained spectra of the quasar with the same instrumental setup, but the seeing was significantly worse. That night, we did obtain spectra of the Landolt standard PG1121+145, which we used to derive an approximate photometric calibration for our quasar spectra. Figure 4 shows the calibrated spectra of the combined A/B components and of star c.

We identified a series of heavy-element absorption lines in the quasar spectrum that correspond well with C III], Fe II and Mg II at $z \approx 0.83$ (see Figure 4). Table 4 lists the identified lines with their wavelengths and estimated equivalent widths. The equivalent width is typical of Mg II absorption systems (Steidel & Sargent 1992) over a wide range of redshifts and impact parameters (e.g. Steidel, Dickinson & Persson 1994, Churchill, Steidel & Vogt 1996). While the absorption redshift is a plausible lens redshift (see §4), such absorption systems are common in unlensed quasars and we cannot regard it as evidence in support of the lensing hypothesis. Steidel et al. (1994) and Churchill et al. (1996) have found, however, that the galaxies responsible for Mg II absorption systems are usually detectable, and in our images there is a plausible, faint candidate galaxy 2.2' SW of component A with $m_I \sim 21$ (see Figure 2). The candidate galaxy is not clearly observed in the B or R images. The implied impact parameter of $9h^{-1}$ kpc is typical of Mg II absorption system galaxies with the observed equivalent width.

We also combined the spectra of the similar redshift quasars 1257+3439, 1356+5806, and 2340+0019 (Steidel & Sargent 1992) with spectra of a K4 dwarf and a K4 giant star scaled to the observed continuum ratios (the results are insensitive to variations of spectral type between K3 and K5). The stars have a broad MgIb absorption feature near 5000-5300 Å which is prominent even when added to the spectrum of the quasar. The absence of the feature in the observed spectrum (Figure 4) is further evidence that component B cannot be a star.

The poor seeing at the time we obtained the spectrum makes it very difficult to separate the two objects. We attempted to do so by modeling the spatially resolved data with a flat background and two positive definite spectra with the photometrically-determined separation, convolved with a Gaussian seeing profile. Experiments with the spectrum of star c demonstrated that our model would extract a spectrum matching the one obtained by standard methods shown in Figure 3, and experiments with Monte Carlo simulations of the quasar components demonstrated that the extraction procedure would not seriously contaminate the emission line properties of the two components given the separation, seeing, and noise properties of the data. We forced the extracted spectra to match the observed B , R , and narrow band flux ratios to reduce the ambiguities in the solution. The residuals for fitting the A/B components are not as good as the residuals when we modeled the spectrum of star c, particularly in the V band region where we lacked photometric constraints. Figure 5 shows the resulting spectra for A and B. The results are most reliable in the region near the narrow band filters, moderately reliable in the region near the broad band B and R filters, and of dubious reliability elsewhere. The region from the red edge of the B band through the V band is particularly problematic, since the HeII, OIII], and CIII] lines appear mainly in the estimated spectrum of A, the MgII absorption feature appears

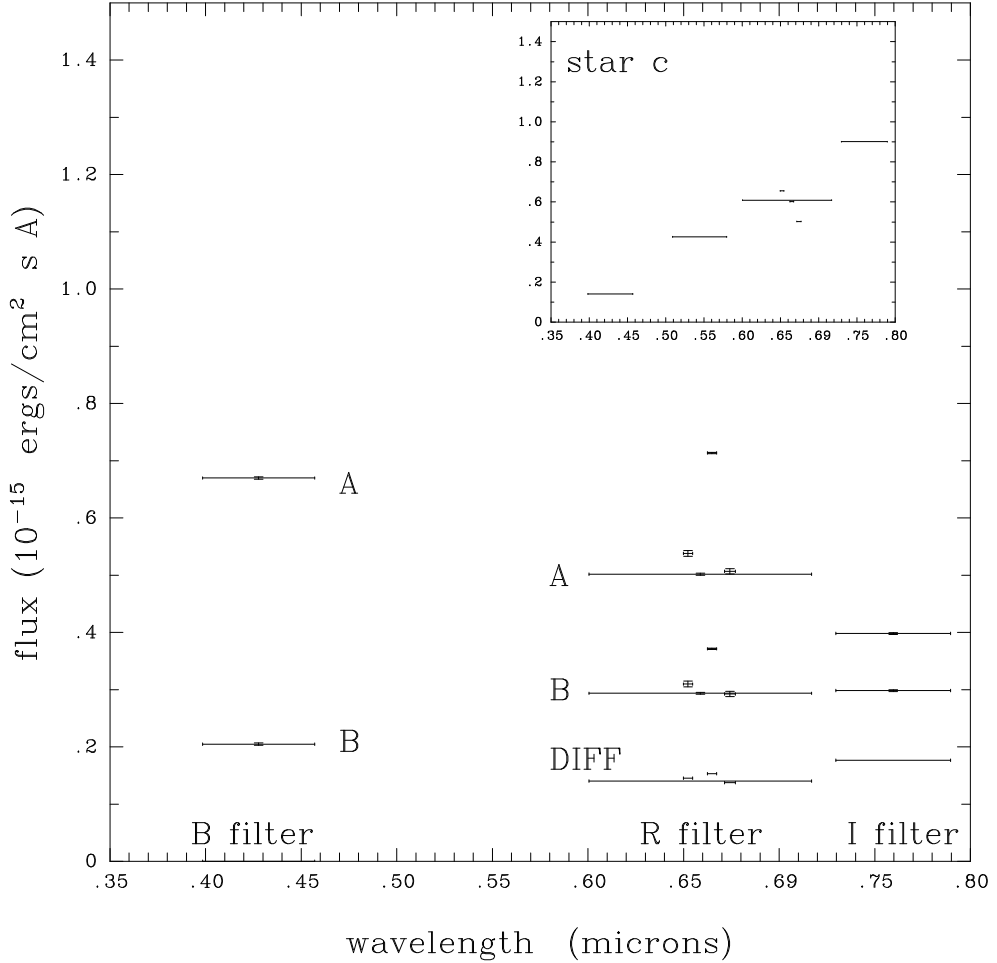


Fig. 3.— Narrow-band photometry of the separate A and B components estimated from the calibrated spectrum and the photometry. The inset shows the analogous measurements for star c. The error bars in wavelength show the rms width of the filter, and the error bars in flux represent the uncertainty in the relative fluxes from the photometry. The DIFF values show the residuals after scaling the A component photometry to the *B*-filter flux of component B and subtracting. The *I* filter averages are truncated before the red edge of the passband because the calibrated spectrum ends at 8000 Å.

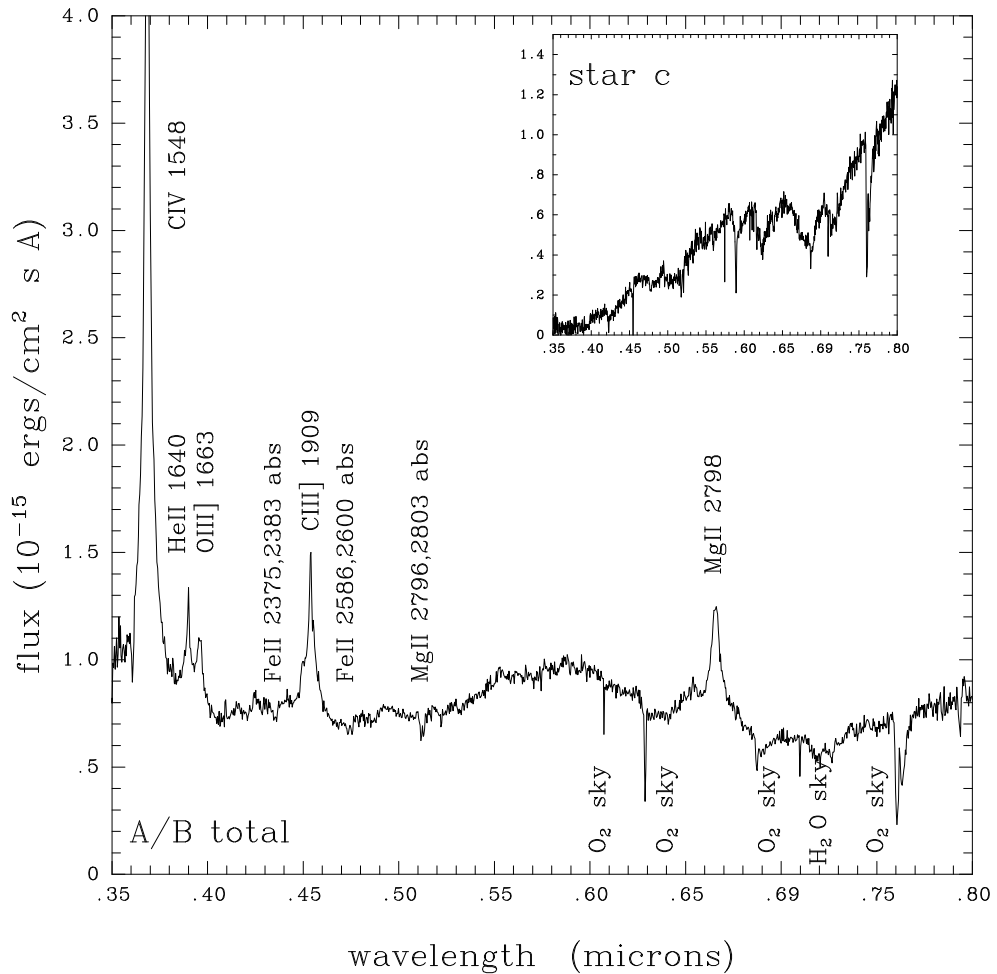


Fig. 4.— The calibrated spectrum of the combined A/B components. The inset shows the calibrated spectrum of star c. The $z_{abs} = 1.33$ C IV doublet lies just inside the left edge.

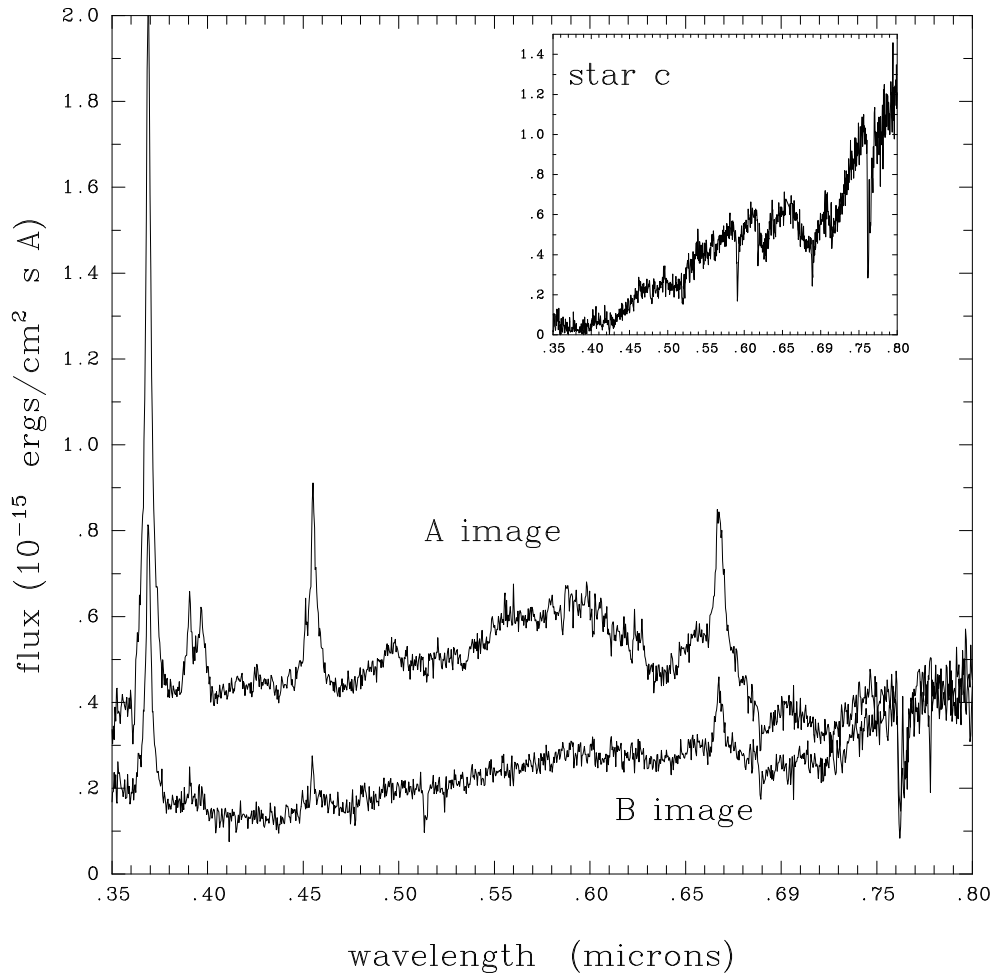


Fig. 5.— Estimated spectra of the A and B components. The spectra are most reliable near the Mg II line because of the additional constraints from the narrow band photometry. There are significant unmodeled residuals in the region with the poorly split OIII] and CIII] emission lines and MgII absorption line.

mainly in the spectrum of B, and there are significant unmodeled residuals.

4. Interpretation

We believe that component B is not a star for three reasons. First, the MgII 2798 Å line is present in both components based either on the narrow band photometry or the spectral reconstruction. Second, the spectral reconstruction, while not ideal, generally required emission lines in both objects, particularly in the regions where the model was stabilized by the broad band photometry. Third, K stars should produce a broad absorption feature in the combined (A + B) spectrum that we do not observe. If both objects possess broad emission lines with comparable redshifts, the two plausible explanations are that the object is a gravitational lens or that it is the smallest-separation binary quasar yet found.

Using the procedures of Kochanek (1992) we estimate that the relative probabilities of finding two lensed or correlated quasars with the observed separation and magnitude difference are approximately $p_{lens} \sim 0.02$ and $p_{corr} \sim 10^{-8}$. The probability that the system is a lens is overwhelmingly favored because quasars as bright as SBS 0909+532 A, B have very low space densities. Although the velocity difference is consistent with zero within our estimates for random errors, we cannot sensibly derive any limits due to the systematic effects on our estimates of the separate spectra in §3. The projected separation of the two quasars, if they are distinct objects, is only $4.7h^{-1}$ kpc (for $\Omega_0 = 1$). All other multiple quasar systems with such small separations are lenses, while the smallest binary quasar known not to be a lens is PKS 1145–071 ($\Delta\theta = 4.^{\circ}2$, $\Delta m = 0.8$, $z = 1.35$, Djorgovski et al. 1987) with a projected separation of $18h^{-1}$ kpc. The broad band color differences are, however, only easily explained for a binary quasar.

The only obstacles to explaining the SBS 0909+532 A/B system as a lensed pair are differences in the spectra of the two objects. In a gravitational lens, spectral differences can be produced by time delays, microlensing, emission by the lens galaxy, and extinction by the lens galaxy. Time delays and microlensing are unlikely to produce a difference in the spectra of the breadth in wavelength and amplitude of flux that is observed as an apparent reddening of B. For a standard extinction curve to produce the measured spectral differences, component B must have $E(B - V) \simeq 0.43$ more extinction than component A, and the intrinsic flux ratio must be -0.58 mags (B is intrinsically brighter than A). If the spectral differences are due to the presence of a lens galaxy, then we expect the blue flux ratio to be the best estimate of the true flux ratio because it is dominated by the broad CIV (1549 Å) emission line. If we scale the photometry of A to match the *B*-filter flux of component B, and subtract, the residuals no longer have a CIV line feature in the narrow

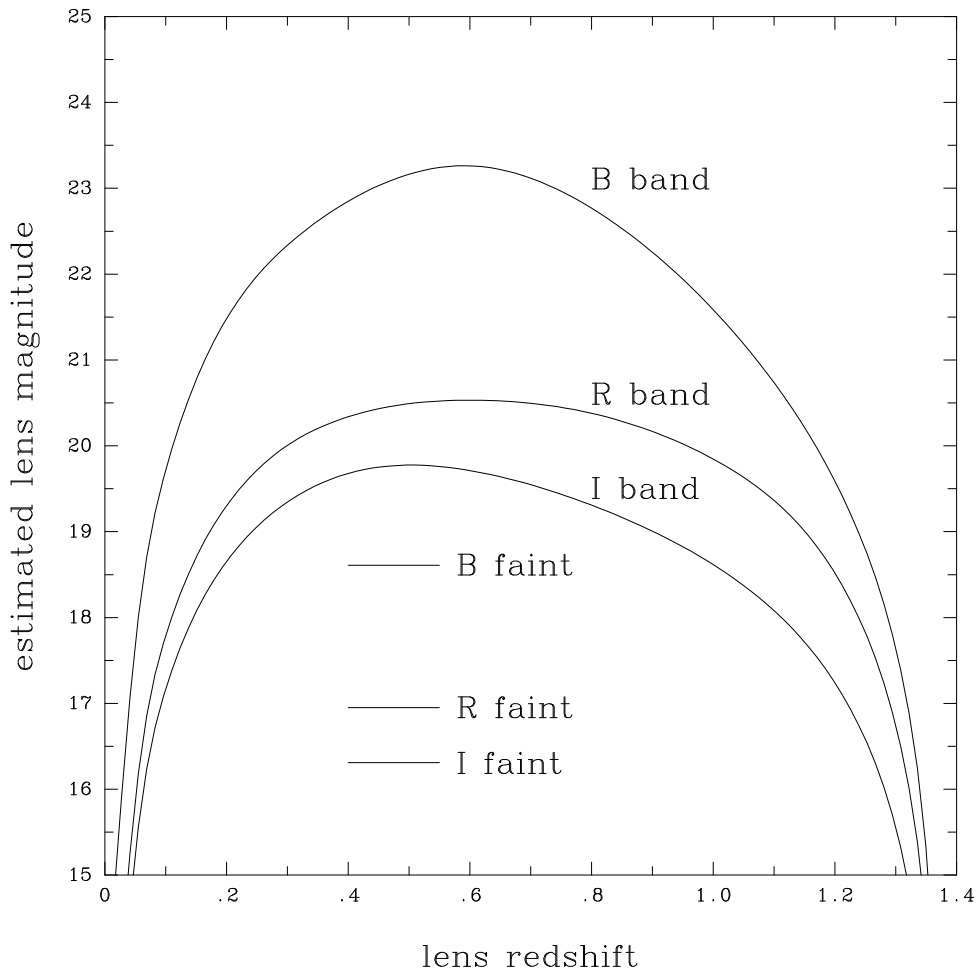


Fig. 6.— Estimated magnitude of a lens galaxy as a function of the lens redshift, assuming the lens is an elliptical galaxy. Horizontal bars indicate the magnitude of the faint component in each broad band filter.

band photometry (see Figure 4). In any other scenario (B not a quasar, flux differences due to reddening, two different quasars) such a cancellation would be a remarkable chance coincidence. The estimated magnitude of the galaxy is then $I \sim 17$ mag, and the flux of the galaxy is a substantial fraction of the total flux attributed to component B. However, Monte Carlo simulations show that such a bright galaxy would produce detectable residuals in our data.

If we assume an SIS lens model, we can estimate the lens redshift and magnitude using the procedures of Kochanek (1992). For $\Omega = 1$ the mean redshift is $\langle z_l \rangle = 0.50 \pm 0.20$, and 90% of the probability lies between $0.18 < z_l < 0.83$. The luminosity of the lens galaxy is $L/L_* = (\Delta\theta/\Delta\theta_*(1-x))^{2/\gamma}$ where $x = D_{LS}/D_{OS}$, D_{LS} and D_{OS} are angular-size distances from the lens and the observer to the source, respectively, $\Delta\theta_* = 2.^{\circ}92(\sigma_*/225 \text{ km s}^{-1})^2$ is the splitting scale for an L_* galaxy, σ_* is the corresponding velocity dispersion, and $\gamma \simeq 4$ is a “Tully-Fisher” exponent. Figure 6 shows the expected magnitude of the lens galaxy assuming an L_* elliptical galaxy has absolute luminosity $B_* = -19.9 + 5 \log h$ mag and the K-corrections and evolution models of Guiderdoni & Rocca-Volmerange (1988). A galaxy with $I \simeq 17$ is also predicted to have a lens redshift of $z_l \simeq 0.1$, significantly below the 90% confidence range for the lens redshift.

Our case for SBS 0909+532 remains somewhat circumstantial due to the limitations of the data. Refining our results requires spectra in the good seeing conditions that consistently eluded us, and higher-resolution images. The identification of a lens may be the simplest means of resolving the question, because the lens interpretation appears to require a bright lens galaxy. We intend to carry out infrared observations to search for such a galaxy to take advantage of both better imaging conditions, and reduced quasar-galaxy contrast.

Acknowledgements: We thank Paul Schechter and Craig Foltz for helping us obtain data on the SBS 0909+532 system. We also thank the KPNO staff, particularly Ed Carder, for lending us the narrow band filters used in §2. We thank B. McLeod for checking several photometric results using methods independent of Daophot, and C. Keeton for checking the evolution model. A. Dobrzański is supported by NASA contract NAS8-39073. The Hamburg Bright Quasar Survey is supported by the DFG through grants Re 353/11 and Re 353/22.

REFERENCES

Burstein, D., & Heiles, C., 1982, AJ 87, 1165

Churchill, C.W., Steidel, C.C., & Vogt, S.S., 1996, ApJ in press

Djorgovski, S., Perley, R., Meylan, G., McCarthy, P., 1987, ApJL 321, L17

Engels, D., Dobrzycki, A., Hagen., H.-J., Elvis, M., Huchra, J. P., & Reimers, D., 1996, A&A preprint

Guiderdoni, B., & Rocca-Volmerange, B., 1988, A&AS 74, 185

Kochanek, C.S., 1992, ApJ 384, 1

Kochanek, C.S., 1996, ApJ 466, 638

Kochanek, C.S., Falco, E.E., & Schild, R., 1995, ApJ 452, 109

Steidel, C.C., & Sargent, W.L.W., 1992, ApJS 80, 1

Steidel, C.C., Dickinson, M., & Perrson, S.E., 1994, ApJL 437, L75

Stepanyan, D.A., Lipovetskii, V.A., Chavushyan, V.O., Erastova, L.K., & Shapovalova, A.I., 1991, Astrofizika 34, 1

Stetson, P.B., 1992, J.R.Astron.Soc.Can. 86, 71

Véron-Cetty, M.-P. & Véron, P. 1996, A&AS 115, 97

Table 1: Absolute Photometry

Filter	m_A	m_B	m_a	m_b	m_c
I	16.00 ± 0.03	16.31 ± 0.05	13.54 ± 0.11	14.22 ± 0.04	15.05 ± 0.09
R	16.36 ± 0.04	16.95 ± 0.04	13.94 ± 0.12	14.78 ± 0.05	16.19 ± 0.05
B	17.24 ± 0.03	18.61 ± 0.03	14.79 ± 0.08	16.02 ± 0.02	18.68 ± 0.03

Notes – A and B are the quasar images, and a, b, and c are the reference stars (see Figure 1). The absolute photometry is significantly less accurate than the relative photometry presented in Table 2. The broad band filters are the Kitt Peak I and B filters, and the Schombert R filter.

Table 2: Relative Photometry

Filter	N_{im}	$\Delta\theta$	Δm	Δm_{AB}
<i>I</i>	9	$1.^{\circ}107 \pm 0.^{\circ}006$	0.313 ± 0.010	–
<i>R</i>	8	$1.^{\circ}109 \pm 0.^{\circ}005$	0.581 ± 0.010	$\equiv 0$
<i>B</i>	4	$1.^{\circ}111 \pm 0.^{\circ}006$	1.286 ± 0.015	–
<i>KP6520</i>	6	$1.^{\circ}104 \pm 0.^{\circ}006$	0.599 ± 0.028	0.018 ± 0.030
<i>KP6649</i>	3	$1.^{\circ}102 \pm 0.^{\circ}001$	0.709 ± 0.005	0.128 ± 0.011
<i>KP6737</i>	3	$1.^{\circ}101 \pm 0.^{\circ}007$	0.596 ± 0.027	0.015 ± 0.028

Notes – N_{im} is the number of images used in the analysis; it includes only images with FWHM better than $1.^{\circ}2$. The errors in the separation $\Delta\theta$ and the flux ratios Δm are the observed dispersion between the images. $\Delta m_{AB} = (m_A - m_B) - (R_A - R_B)$ is the color difference between the quasar images in each band compared to the quasar images in *R*. The position angle of B relative to A is $115^{\circ}2 \pm 0^{\circ}3$ (E of N).

Table 3: Properties of Narrow-band Filters

Filter	λ_c (Å)	FWHM (Å)	$\Delta\lambda$	Peak transmission (%)
<i>KP</i> 6520	6524	70		84
<i>KP</i> 6649	6649	71		87
<i>KP</i> 6737	6743	84		89

Table 4: Absorption Lines

Element	rest λ (Å)	rest W_{\circ} (Å)	z
C IV	1549	2.4	1.33
C III]	1909	1.4	0.833
Fe II	2375	1.0	0.831
Fe II	2383	0.3	0.830
Fe II	2587	0.9	0.831
Fe II	2600	0.5	0.829
Mg II	2796	1.0	0.830
Mg II	2803	0.8	0.830